Nanoscale Research Letters
a SpringerOpen Journal

NANO EXPRESS Open Access

Highly selective fluorescent chemosensor for Zn^{2+} derived from inorganic-organic hybrid magnetic core/shell $Fe_3O_4@SiO_2$ nanoparticles

Yujiao Wang, Xiaohong Peng, Jinmin Shi, Xiaoliang Tang, Jie Jiang and Weisheng Liu*

Abstract

Magnetic nanoparticles with attractive optical properties have been proposed for applications in such areas as separation and magnetic resonance imaging. In this paper, a simple and novel fluorescent sensor of Zn^{2+} was designed with 3,5-di-tert-butyl-2-hydroxybenzaldehyde [DTH] covalently grafted onto the surface of magnetic core/shell $Fe_3O_4@SiO_2$ nanoparticles [NPs] (DTH-$Fe_3O_4@SiO_2$ NPs) using the silanol hydrolysis approach. The DTH-$Fe_3O_4@SiO_2$ inorganic-organic hybrid material was characterized by transmission electron microscopy, dynamic light scattering, X-ray power diffraction, diffuse reflectance infrared Fourier transform, UV-visible absorption and emission spectrometry. The compound DTH exhibited fluorescence response towards Zn^{2+} and Mg^{2+} ions, but the DTH-$Fe_3O_4@SiO_2$ NPs only effectively recognized Zn^{2+} ion by significant fluorescent enhancement in the presence of various ions, which is due to the restriction of the N-C rotation of DTH-$Fe_3O_4@SiO_2$ NPs and the formation of the rigid plane with conjugation when the DTH-$Fe_3O_4@SiO_2$ is coordinated with Zn^{2+}. Moreover, this DTH-$Fe_3O_4@SiO_2$ fluorescent chemosensor also displayed superparamagnetic properties, and thus, it can be recycled by magnetic attraction.

Background

Zinc is the second abundant transition metal ion in the human body, which plays a vital role in various biological processes, such as gene expression [1], apoptosis [2], enzyme regulation [3], and neurotransmission [4,5]. It is also believed that the Zn^{2+} homeostasis may have some bearing on the pathology of Alzheimer's disease and other neurological problems [6-8]. Therefore, there is an urgency to develop approaches to detect Zn^{2+} *in vivo*. Besides, techniques for the separation and removal of metal ions and additives in the detection process are very important to prevent poisoning in environmental and biological fields. Conventional analytical methods including atomic absorption spectrophotometry [9], inductively coupled plasma atomic emission spectrometry [10], and electrochemical method [11] can hardly be applied for Zn^{2+} ion detection in biological systems due to their complicated pretreatment steps and expensive equipment. Hence, for convenience in future *in vivo* applications, various fluorescent probes based on small molecules have been designed. They were fairly efficient as reported [12-22]; however, the small molecules would be toxic [23], and it is impossible to recover or remove them from organisms [24]. The limitation of recoverability blocked the practical applications of small molecular fluorescent probes. To resolve this challenge, the inorganic supports incorporated with small molecular fluorescent probes were applied for the improvement on recoverability.

Various mesoscopic or nanoscopic materials can be acted as the inorganic supports in the design of fluorescent probes, including magnetic nanoparticles, nanotubes, mesoporous silica, metal nanoparticles, and TiO_2 [25-34]. Among all these inorganic materials, magnetic silica core/shell nanoparticles have advantages over other competitors for biological and environmental applications [35-41]. Firstly, they could be simply separated or recovered via external magnetic field. Besides, with magnetic silica core/shell nanoparticles as delivery, their low toxicity and biocompatibility also had advantages for the design of biological fluorescent probes.

* Correspondence: liuws@lzu.edu.cn
Key Laboratory of Nonferrous Metals Chemistry and Resources Utilization of Gansu Province and State Key Laboratory of Applied Organic Chemistry, College of Chemistry and Chemical Engineering, Lanzhou University, Lanzhou, 730000, People's Republic of China

Furthermore, the silica shell around magnetic core has large surface area, and it can be grafted by fluorescent probes. Therefore, to develop nontoxic, biocompatible, and recoverable fluorimetric Zn^{2+} sensors, introducing the magnetic silica nanoparticles with small molecular fluorescent probes incorporated is very necessary and highly desirable.

In this work, we designed and synthesized a magnetic recoverable fluorescence Zn^{2+} sensor based on 3,5-di-tert-butyl-2-hydroxybenzaldehyde [DTH] covalently grafted onto Fe_3O_4@SiO_2 nanoparticles [NPs] (DTH-Fe_3O_4@SiO_2) to provide highly selective fluorescence changes and efficient magnetic recoverability (Figure 1). This Zn^{2+}-selective fluorescent switch of the immobilized chemosensors displayed excellent reversibility, combined with its superparamagnetic property, enabling the recovery of material and repeated uses for Zn^{2+} sensing.

Experimental details

Materials and methods

All reagents are purchased commercially. Besides, ethanol was used after purification by standard methods. Other chemicals were used as received without further purification.

Thermal gravimetric analysis [TGA] (P.E. Diamond TG/DTA/SPAECTRUN ONE thermal analyzer, PerkinElmer Inc., Waltham, MA, USA), dynamic light scattering (BI-200SM, Brookhaven Instruments Corporation, Holtsville, NY, USA), transmission electron microscopy [TEM] (Tecnai G^2 F30, 300 kV, FEI Company, OR, USA), and energy-dispersive X-ray spectrometer [EDX] were used to characterize the materials. X-ray diffraction [XRD] pattern of the synthesized products was recorded with a Rigaku D/MAX 2400 X-ray diffractometer (Tokyo, Japan) using Cu $K\alpha$ radiation (λ = 0.154056 Å). The scan range (2θ) was from 10° to 80°. Solid-state infrared [IR] using diffuse-reflectance infrared Fourier transform [DRIFT] spectroscopy was performed in the 400- to 4,000-cm^{-1} region using a Bruker Vertex 70v (Bremen, Germany) and IR-grade KBr (Sigma-Aldrich Corporation, St. Louis, MO, USA) as the internal standard. ^{1}H NMR and ^{13}C NMR spectra were measured on a Bruker DRX 400 spectrometer in a $CDCl_3$ solution with TMS as the internal standard. Chemical shift multiplicities are reported as s = singlet, t = triplet, q = quartet, and m = multiplet. Mass spectra were recorded on a Bruker Daltonics esquire6000 mass spectrometer. UV absorption spectra were recorded on a Varian Cary 100 spectrophotometer (Palo Alto, CA, USA) using

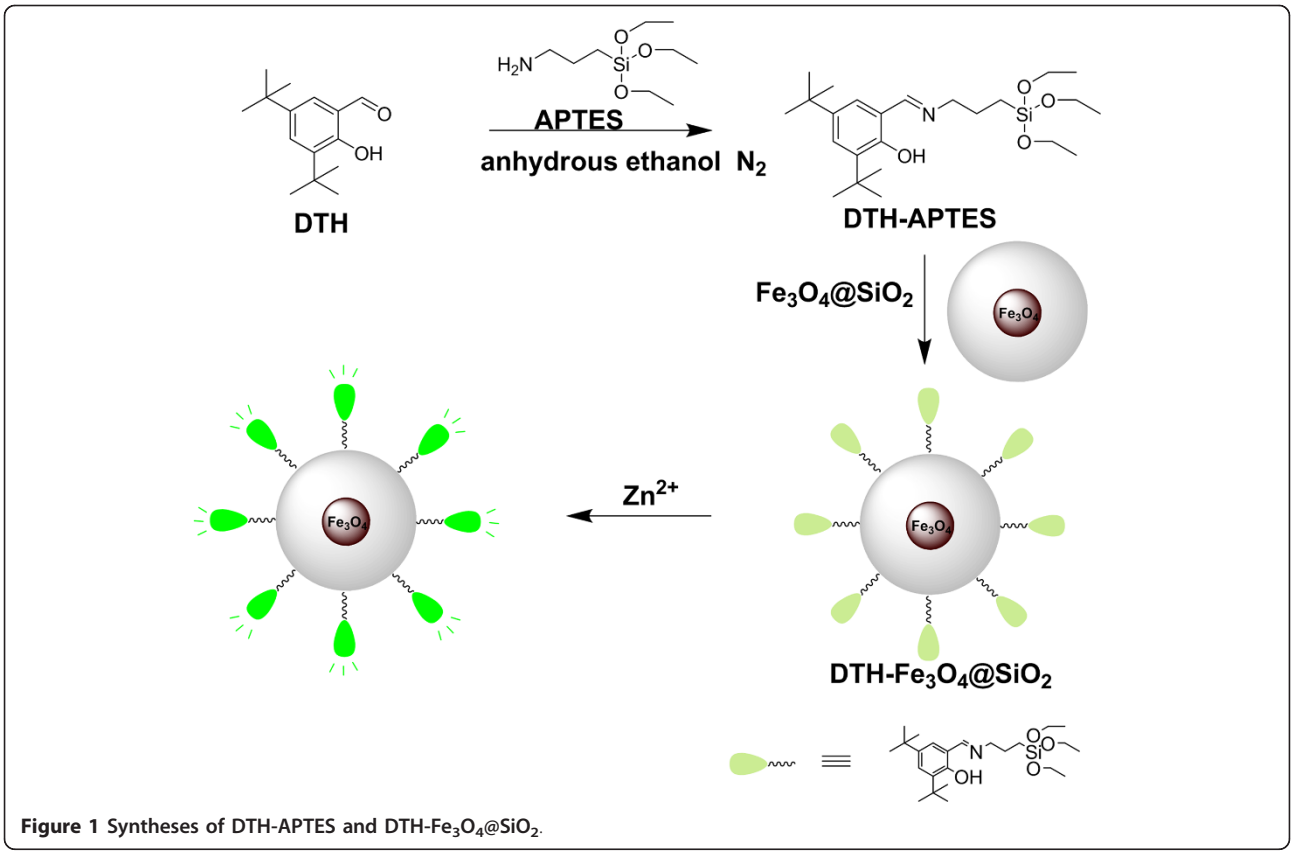

Figure 1 Syntheses of DTH-APTES and DTH-Fe_3O_4@SiO_2.

quartz cells of 1.0-cm path length. Fluorescence measurements were made on a Hitachi F-4500 spectrophotometer (Tokyo, Japan) and a Shimadzu RF-540 spectrofluorophotometer (Chorley, UK) equipped with quartz cuvettes of 1.0-cm path length with a xenon lamp as the excitation source. An excitation and emission slit of 10.0 nm was used for the measurements in the solution state. All spectrophotometric titrations were performed with a suspension of the sample dispersed in ethanol.

Synthesis of Fe_3O_4@SiO_2 NPs

Fe_3O_4@SiO_2 NPs were synthesized according to the study of Nigam et al. [42]. The process can be briefly described in the following two steps: (1) $FeCl_2$ and $FeCl_3$ (molar ratio, 1:2) were added to a concentrated solution of base (25% ammonium hydroxide) under N_2. The solution was mechanically stirred for 1 h at 20°C and then heated at 70°C for 1 h. The mixture was then stirred for 30 min at 90°C upon addition of citric acid (0.5 g/ml). After cooling the reaction mixture to room temperature, the magnetite NPs were obtained by permanent magnet, and then it was rinsed with deionized water to remove excess citric acid and other nonmagnetic particles thoroughly. (2) Then, the magnetite NPs were further coated with a thin silica layer via a modified Stöber method [43] to obtain stable Fe_3O_4@SiO_2. Tetraethyl orthosilicate was hydrolyzed with magnetic NPs as seeds in an ethanol/water mixture. The resulting silica-coated magnetite NPs with an average diameter of 60 to 70 nm were used.

Synthesis of DTH-Fe_3O_4@SiO_2 NPs

As shown in Figure 1, the synthetic procedure for 2,4-di-tert-butyl-6-((3-(triethoxysilyl)propylimino)methyl) phenol [DTH-APTES] followed the method previously described in the literatures [44,45]. DTH (234 mg, 1 mmol) and (3-aminopropyl) triethoxysilane [APTES] (221 mg, 1 mmol) were mixed in dry ethanol (15 mL) at room temperature. Then, the solution was refluxed for 3 h under N_2. After that, the solvent was evaporated, and the crude product was further purified by flash column chromatography (silica gel, ethyl acetate/petroleum ether 1:2) to produce 371 mg (84.9%) of DTH-APTES as yellow oil. ESI-MS: *m/z* 438.5 ($M + H^+$). ^{1}H NMR: (400 MHz, $CDCl_3$): δ (ppm) 0.69 (t, 2H, CH_2Si); 1.22 (t, 9H, CH_3); 1.30 (s, 9H, $C(CH_3)_3$); 1.43 (s, 9H, $C(CH_3)_3$); 1.82 (m, 2H, CH_2); 3.58 (t, 2H, NCH_2); 3.82 (q, 6H, $SiOCH_2$); 7.07, 7.36 (d, 2H, Ar); 8.34 (s, 1H, HC = N). ^{13}C NMR (100 MHz, $CDCl_3$): 7.92 (CH_2Si); 18.30 (CH_3); 24.38, 29.40, 29.70, 31.50 (CH_3); 34.11 (C), 35.01 (C); 58.41 (CH_2); 62.08 (CH_2); 117.83, 125.69, 126.66, 136.65, 139.75, 158.27 (Ar); 165.80 (C = N). FT-IR (KBr pellet) (cm^{-1}): 1,637 ($\nu_{C=N}$), 1,275-1,252 (ν_{C-O}), 1,596-1,342 ($\nu_{C=C}$), 1,106-1,085 (ν_{Si-O}).

One hundred milligrams of dried Fe_3O_4@SiO_2 NPs and 356 mg (0.81 mmol) of DTH-APTES were suspended in 10 mL of anhydrous ethanol. The mixture was refluxed for 8 h at 80°C under N_2 to obtain DTH-Fe_3O_4@SiO_2. The nanoparticles were collected by centrifugation and repeatedly washed with anhydrous ethanol thoroughly. Unreacted organic molecules were removed completely and monitored by the fluorescence of the upper liquid. Then, the DTH-Fe_3O_4@SiO_2 NPs were finally dried under vacuum over night. About 2.81% DTH-APTES in the precursors was finally grafted on the NPs, and the rest could be recycled if no hydrolysis occurred.

Results and discussion

Characterization of DTH-Fe_3O_4@SiO_2

The TEM image (Figure 2A) of DTH-Fe_3O_4@SiO_2 reveals that iron oxide NPs have entrapped in the silica shell successfully, in which the core/shell structures are in a narrow size distribution of 60 to 70 nm [46,47], and the diameter of the magnetic core is about 10 nm. The weight ratio of iron vs. silicon was measured to be 2.63:38.94 by EDX. Hence, according to TGA, each magnetic NP has about 6,000 DTH-APTES molecules grafted (see Additional file 1). More importantly, the right size of magnetic core/shell NPs smaller than 100 nm is an advantage for their good dispersibility. In addition, an inert silica coating on the surface of magnetite nanoparticles prevents their aggregation in liquid [48]. Hence, such a good performance on the dispersibility can improve their chemical stability and provide better protection against toxicity.

In addition, dynamic light scattering [DLS] was performed to further reveal the colloidal stability of NPs. According to DLS results (Figure 2B), DTH-Fe_3O_4@SiO_2 presents good stabilization and a narrow size distribution with peak centered at 147 nm, confirming its good stabilization in ethanol. In a common sense, the diameter achieved by DLS is mostly higher than the one observed in TEM since the size of NPs identified by DLS includes the grafted molecules' steric hindering and the hydrodynamic radius of first few solvent layers [49-51]. Besides, according to the calculated size of DTH-APTES which covalently grafted on the surface of Fe_3O_4@SiO_2, the grafted molecules' steric hindering could increase the diameter by about 2.72 nm.

Figure 3 shows the XRD powder diffraction patterns of two NPs for the identification of Fe_3O_4 in core/shell NPs. XRD patterns of the synthesized Fe_3O_4@SiO_2 (a) and DTH-Fe_3O_4@SiO_2 (b) display relative diffraction peaks in the 2θ region of 10° to 80°. We could find that XRD patterns show very low intensities for the peaks attributed to the Fe_3O_4 cores, due to the coating of

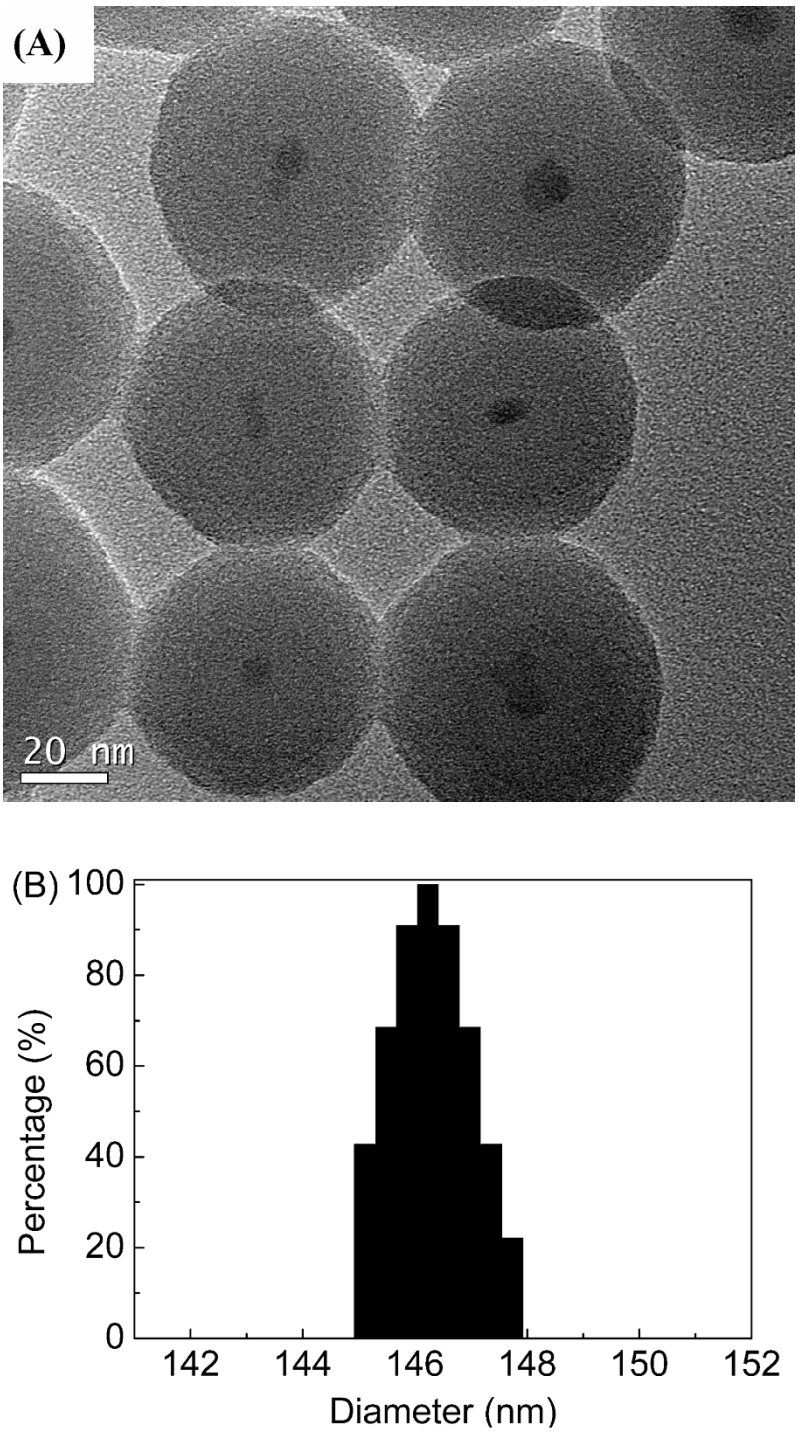

Figure 2 TEM image (A) and the particle size histogram from DLS (B) of DTH-Fe_3O_4@SiO_2.

amorphous silica shell, which deduced the efficient content of Fe_3O_4 cores and then affected the peak intensities. However, the diffraction peaks of DTH-Fe_3O_4@SiO_2 still maintain the same position as the magnetite core (Figure S1 in Additional file 1) [52]. The six characteristic diffraction peaks in Figure 3 can be indexed to (220), (311), (400), (422), (511), and (440), which well agree with the database of magnetite in the

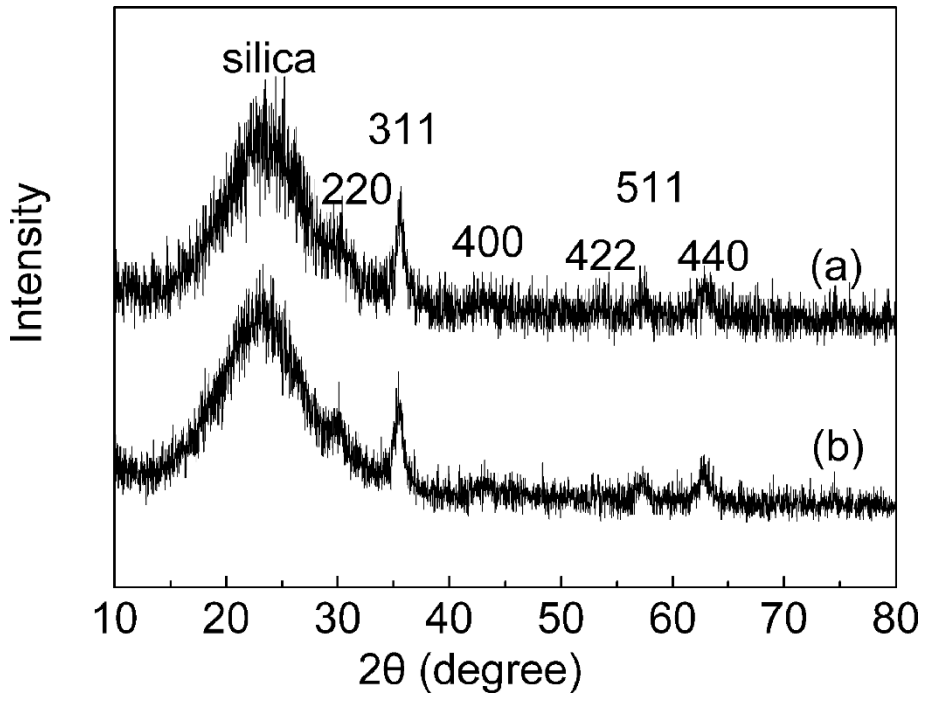

Figure 3 XRD patterns of Fe_3O_4@SiO_2 (a) and DTH-Fe_3O_4@SiO_2 (b).

Joint Committee on Powder Diffraction Standards [JCPDS] (JCPDS card: 19-629) file [42,46,53,54]. Also, the broad XRD peak at a low diffraction angle of 20° to 30° corresponds to the amorphous-state SiO_2 shells surrounding the Fe_3O_4 NPs [53].

The successful conjugation of DTH onto the surface of the Fe_3O_4@SiO_2 NPs can be confirmed by DRIFT (Figure 4). The bands at 3,400 to 3,500 cm^{-1} and 1,000 to 1,250 cm^{-1} are due to -OH stretching on silanol [55]. It indicates that not all the silanol on Fe_3O_4@SiO_2 NPs

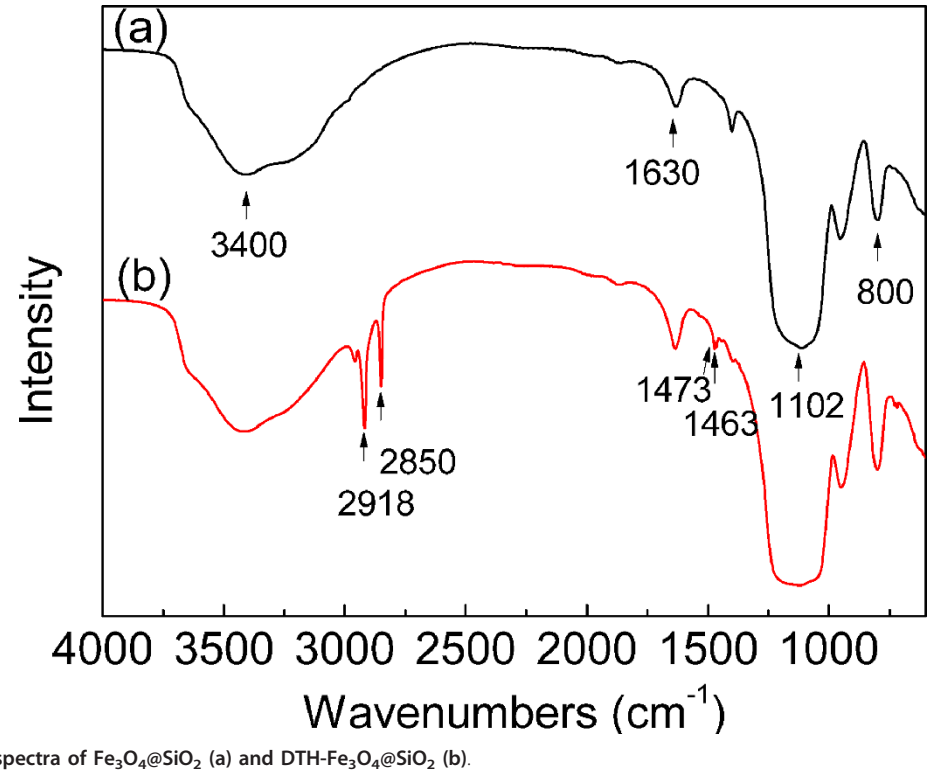

Figure 4 DRIFT spectra of Fe_3O_4@SiO_2 (a) and DTH-Fe_3O_4@SiO_2 (b).

have been covalently modified. The band at 1,630 cm^{-1} represents the bending mode of -OH vibrations [56]. DTH-Fe_3O_4@SiO_2 (see Figure 1) has additional peaks at 2,918 and 2,850 cm^{-1} that correspond to the -CH vibration of aliphatic and aromatic groups [28,57,58]. The bands at 1,473 and 1,463 cm^{-1} of DTH-Fe_3O_4@SiO_2 are probably due to the bending vibrations of -CH_3, which come from the DTH part [59]. According to the spectra of Fe_3O_4@SiO_2 and DTH-Fe_3O_4@SiO_2, the bands which appear as broad and strong and are centered at 1,102 (ν_{as}) and 800 cm^{-1} can be attributed to the siloxane (-Si-O-Si-) [60]. These results support the presence of the organic DTH-APTES in the magnetic material DTH-Fe_3O_4@SiO_2.

The UV-visible [UV-Vis] spectra of DTH-APTES (1.0×10^{-5} M), Fe_3O_4@SiO_2 (0.3 g/L), and DTH-Fe_3O_4@SiO_2 (0.3 g/L) can provide further evidence on the grafting of DTH onto the surface of the Fe_3O_4@SiO_2 NPs (Figure 5). Compared to Fe_3O_4@SiO_2 (b), a new absorption band centered at about 330 nm of DTH-Fe_3O_4@SiO_2 can be attributed to the typical electronic transition of an aromatic ring and -C = N- conjugate system in a Schiff base molecule [29]. This result can also imply the successful immobilization of DTH-APTES onto the magnetic core/shell NPs.

The superparamagnetic property of the magnetic NPs plays a vital role for its biological application. Figure 6 shows the magnetization curves of the Fe_3O_4@SiO_2 and DTH-Fe_3O_4@SiO_2 which were investigated with a vibrating sample magnetometer tuned from -15,000 to 15,000 Oe at 300 K. The result was consistent with the conclusion that magnetic Fe_3O_4 NPs smaller than 30 nm are usually superparamagnetic at room temperature [47]. The saturation magnetization value for synthesized DTH-Fe_3O_4@SiO_2 is about 3.96 emu/g. The saturation magnetization value for Fe_3O_4@SiO_2 support was measured to be 4.24 emu/g. Considering the grafting rate of 7.64% (according to TGA, Figure S2 and Table S1 in Additional file 1), the difference of saturation magnetization values between DTH-Fe_3O_4@SiO_2 and its support could be due to the decreased weight ratio of magnetic support after grafting. More importantly, from the hysteresis loops of Fe_3O_4@SiO_2 NPs and the DTH-Fe_3O_4@SiO_2 NPs, it can be found that both exhibited superparamagnetic properties for no remanence was observed when the applied magnetic field was removed. These phenomena were due to the fact that the magnetite core is smaller than 30 nm in core/shell NPs (Figure 2A). As a result of this superparamagnetic property, DTH-Fe_3O_4@SiO_2 had a reversal magnetic responsivity. It could be easily separated from dispersion after only 5 min using a magnet (Figure 6, inset) and then redispersed by mild agitation when the magnet was removed. The reversal magnetic responsivity of DTH-Fe_3O_4@SiO_2 would be a key factor when evaluating their recoverability [61]. The magnetic separation capability of DTH-Fe_3O_4@SiO_2 NPs and the reversibility of the combination between DTH-Fe_3O_4@SiO_2 and Zn^{2+} could also provide a simple and efficient route to separate Zn^{2+} rather than through filtration approach (see Figure 6 inset).

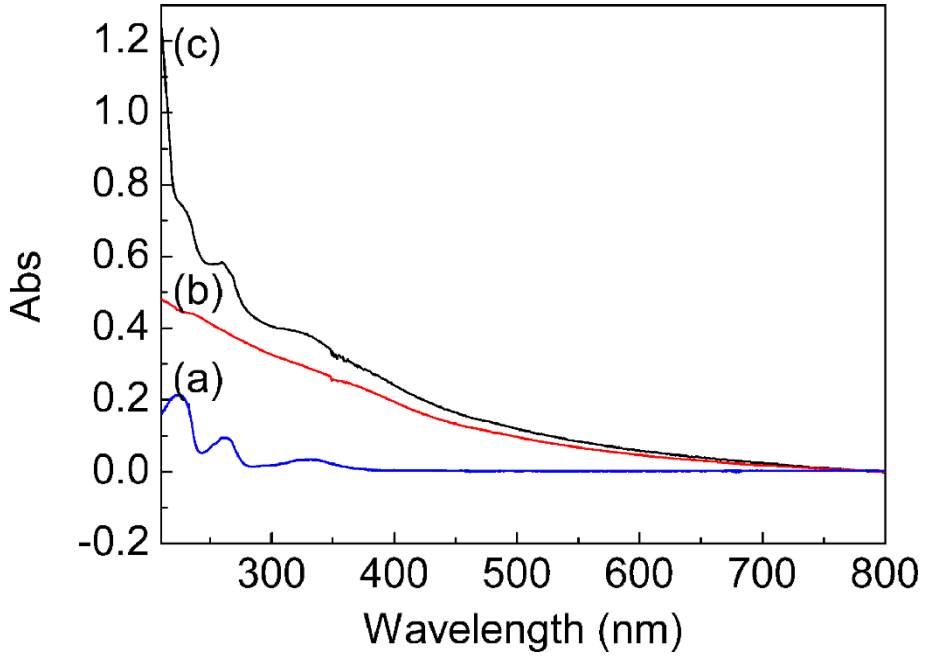

Figure 5 UV-Vis spectra of DTH-APTES (a), Fe_3O_4@SiO_2 (b), and DTH-Fe_3O_4@SiO_2 (c).

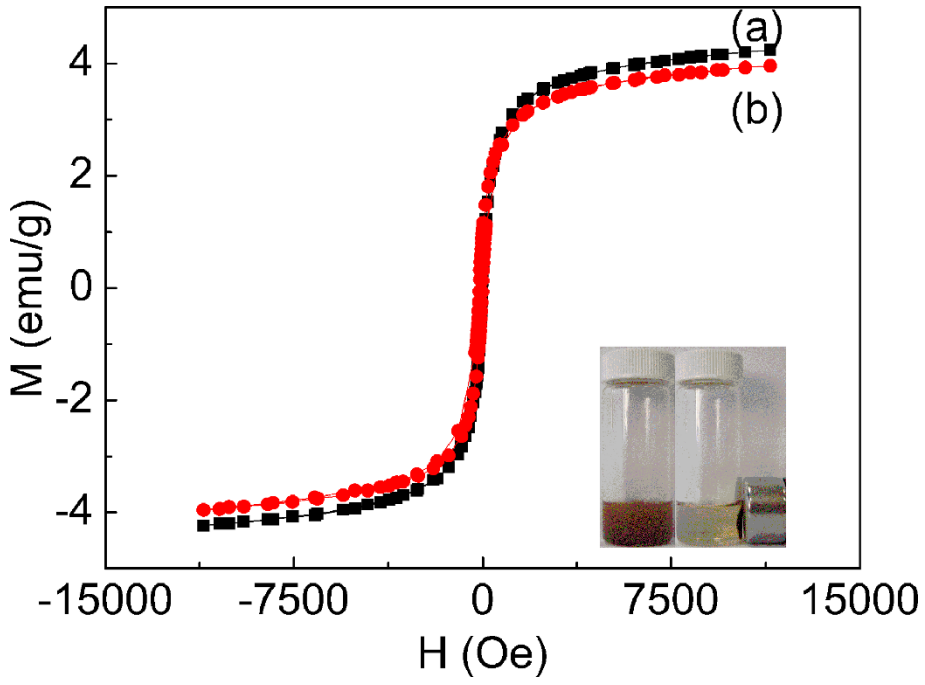

Figure 6 Magnetization curves of the Fe_3O_4@SiO_2 (a) and DTH-Fe_3O_4@SiO_2 (b). Inset shows that DTH-Fe_3O_4@SiO_2 was dispersed to an external magnet in ethanol.

Fluorescence response of DTH-Fe_3O_4@SiO_2

To verify its fluorescence response towards various metal ions, we investigated fluorescence properties of DTH-Fe_3O_4@SiO_2 NPs (0.3 g/L, containing 5.2×10^{-5} M DTH-APTES according to TGA in Figure S2 and Table S1 in Additional file 1) towards various metal ions Ag^+, Ca^{2+}, Cd^{2+}, Co^{2+}, Cr^{3+}, Cu^{2+}, Fe^{3+}, Hg^{2+}, K^+, Mg^{2+}, Mn^{2+}, Na^+, Ni^{2+}, and Zn^{2+} in ethanol solution (all as perchlorates, 1.0×10^{-4} M). As shown in Figure 7A, DTH-Fe_3O_4@SiO_2 NPs exhibited significant 'off-on' changes in fluorescence emission only for Zn^{2+}, but not for the others. It is noted that Cd^{2+} with a d^{10} electron configuration, which often exhibited coordination properties similar to Zn^{2+} [19], do not influence the fluorescence intensity of DTH-Fe_3O_4@SiO_2 NPs significantly. As a comparison, DTH (1.0×10^{-5} M) exhibited fluorescence response towards both Zn^{2+} and Mg^{2+} ions (1.0×10^{-4} M) in the same solution, which is not as selective as DTH-Fe_3O_4@SiO_2 for Zn^{2+} detection (Figure 7B). Compared to the single aldehyde DTH, the origin of selectivity for DTH-Fe_3O_4@SiO_2 may come from its Schiff base structure, which prefers to coordinate with Zn^{2+} under the interference of Mg^{2+}.

The remarkable increase of fluorescence intensity can be explained as follows: DTH-Fe_3O_4@SiO_2 is poorly fluorescent due to the rotation of the N-C bond of DTH-APTES part. When stably chelated with Zn^{2+}, the N-C rotation of DTH-APTES part is restricted and the rigid plane with conjugation is formed and the fluorescence enhanced, which consists of our previous work [62]. The emission spectra of DTH-Fe_3O_4@SiO_2, which is excited at 397 nm, exhibit the emission maximum at 452 nm with a low quantum yield (Φ = 0.0042) at room temperature in ethanol. Upon the addition of excess Zn^{2+}, the fluorescence intensity of DTH-Fe_3O_4@SiO_2 increased by more than 25-fold, the emission maximum shifts from 452 to 470 nm, and the quantum yield (Φ = 0.11) results in a 26-fold increase.

As illustrated in Figure 8A, the fluorescence emission of DTH-Fe_3O_4@SiO_2 (0.3 g/L) increases gradually when adding various concentrations (0 to 30 μM) of Zn^{2+} in ethanol, indicating that Zn^{2+} is quantitatively bound to the Schiff base moiety attached to the NPs. Fluorescence titration experiment suggests that the association constant (K_d) for Zn^{2+} binding to DTH-Fe_3O_4@SiO_2 is calculated to be 51.08 M^{-2} (log K = 1.71; Figure 8A). Job's plot suggested a 1:2 binding ratio for Zn^{2+} with DTH-APTES (Figure 8B).

The competition experiments indicated that the presence of most metal ions, especially Na^+, K^+, Ca^{2+}, and Mg^{2+}, which are abundant in the biological environment, had a negligible effect on Zn^{2+} sensing (Figure 9A). Since Cr^{3+}, Cu^{2+}, Fe^{3+}, and Hg^{2+} also appeared to bind DTH-Fe_3O_4@SiO_2 sensors (Figure S3 in Additional file 1), they quenched the fluorescence of the Zn^{2+}-DTH-Fe_3O_4@SiO_2, owing to an electron or energy transfer between the metal

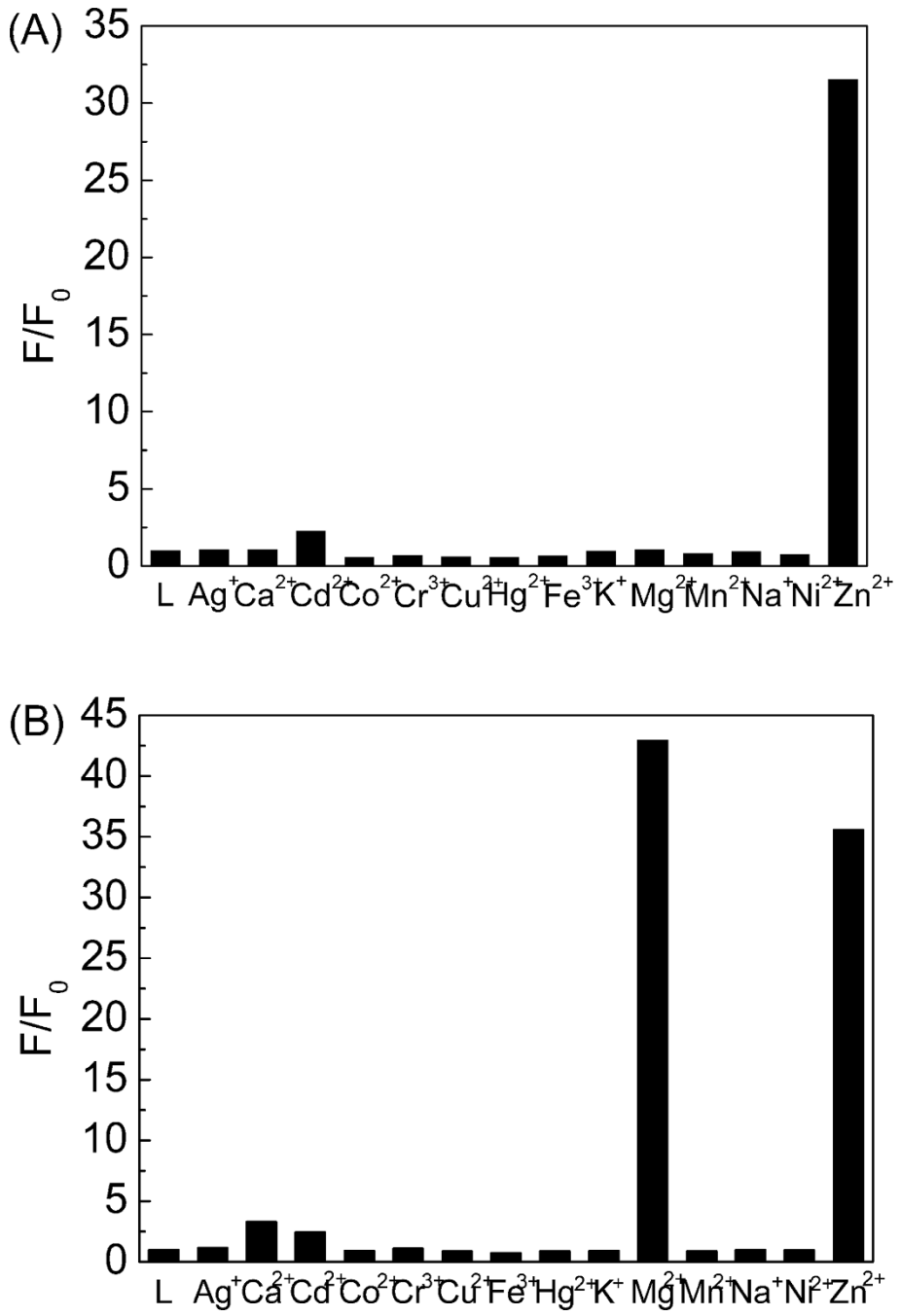

Figure 7 Fluorescence response of DTH-Fe_3O_4@SiO_2 (A) and DTH (B) to various cations. Excitation wavelength was 397 nm. Spectra were recorded every 25 min after adding Zn^{2+}.

cation and fluorophore known as the fluorescence quenching mechanism [63-66]. The fluorescence enhancement that occurred upon exposure to Zn^{2+} was fully reversible as the addition of EDTA (2.5×10^{-4} M; Figure 9B and inset) restored the emission band. Combined with its magnetic property, the results above implied that DTH-Fe_3O_4@SiO_2 was considerably applicable to some field as a new inorganic-organic hybrid sensor for the Zn^{2+} ion.

Figure 10A depicts the UV-Vis spectra of DTH-APTES (10 μM), DTH-APTES (10 μM) + Zn^{2+} (100 μM), DTH-Fe_3O_4@SiO_2 (0.3 g/L), and DTH-Fe_3O_4@-SiO_2 (0.3 g/L) + Zn^{2+} (100 μM). It can be seen that the absorbance peaks at around 390 nm are formed when Zn^{2+} is added in both DTH-APTES and DTH-Fe_3O_4@-SiO_2 systems. The absorption spectra of DTH-Fe_3O_4@-SiO_2 (0.3 g/L) in the presence of various concentrations

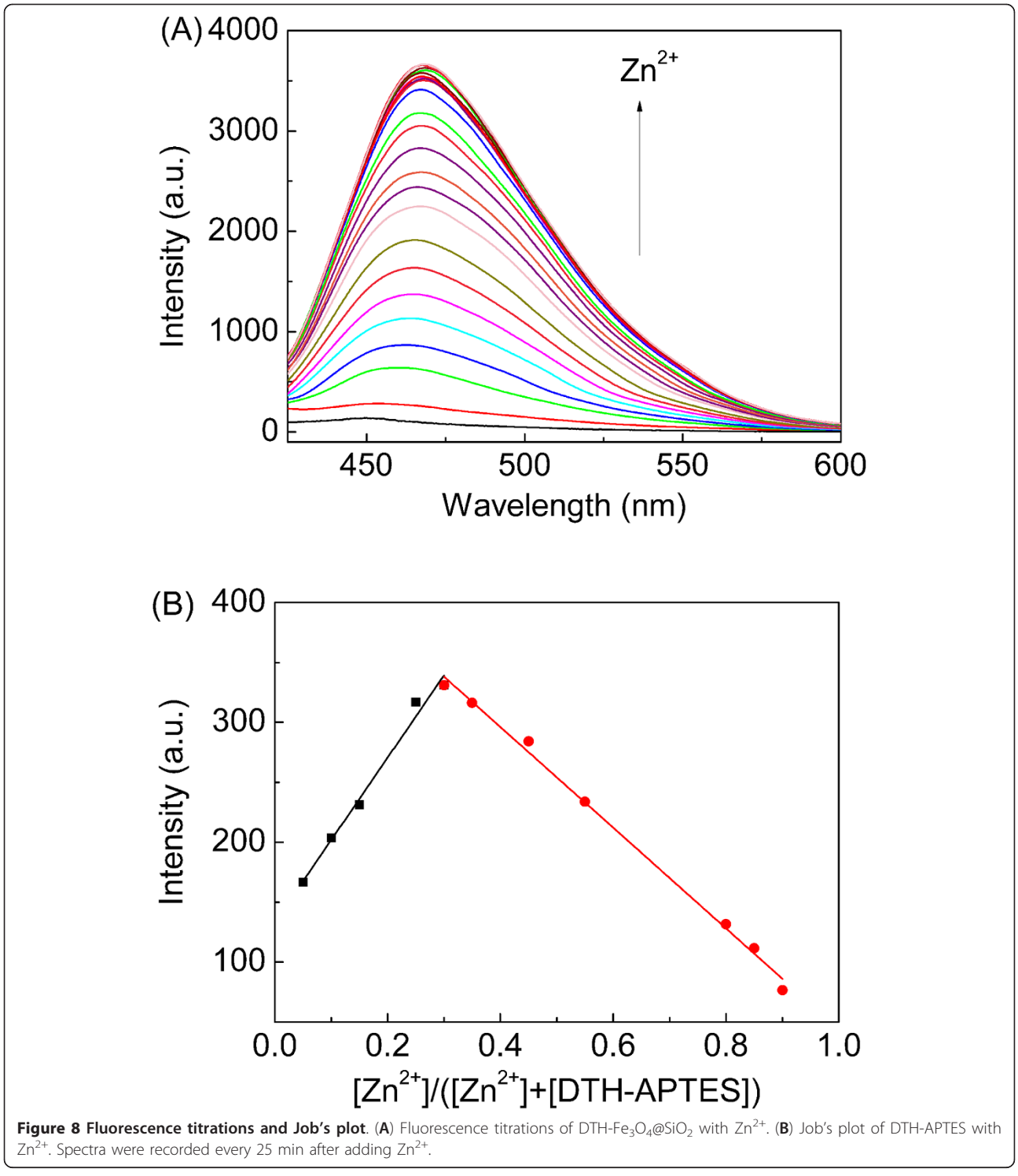

Figure 8 Fluorescence titrations and Job's plot. (**A**) Fluorescence titrations of DTH-Fe_3O_4@SiO_2 with Zn^{2+}. (**B**) Job's plot of DTH-APTES with Zn^{2+}. Spectra were recorded every 25 min after adding Zn^{2+}.

of Zn^{2+} (0 to 240 μM) were investigated in ethanol at room temperature, as shown in Figure 10B. When Zn^{2+} was added gradually, the absorbance of DTH-Fe_3O_4@-SiO_2 at 390 nm gradually increases, which indicated that DTH-Fe_3O_4@SiO_2 NPs coordinated with Zn^{2+} gradually.

Conclusions

In summary, we have successfully designed and synthesized functionalized magnetic core/shell Fe_3O_4@SiO_2 NPs (DTH-Fe_3O_4@SiO_2 NPs) which could act as a new type of fluorescent chemosensor for efficient sensing and

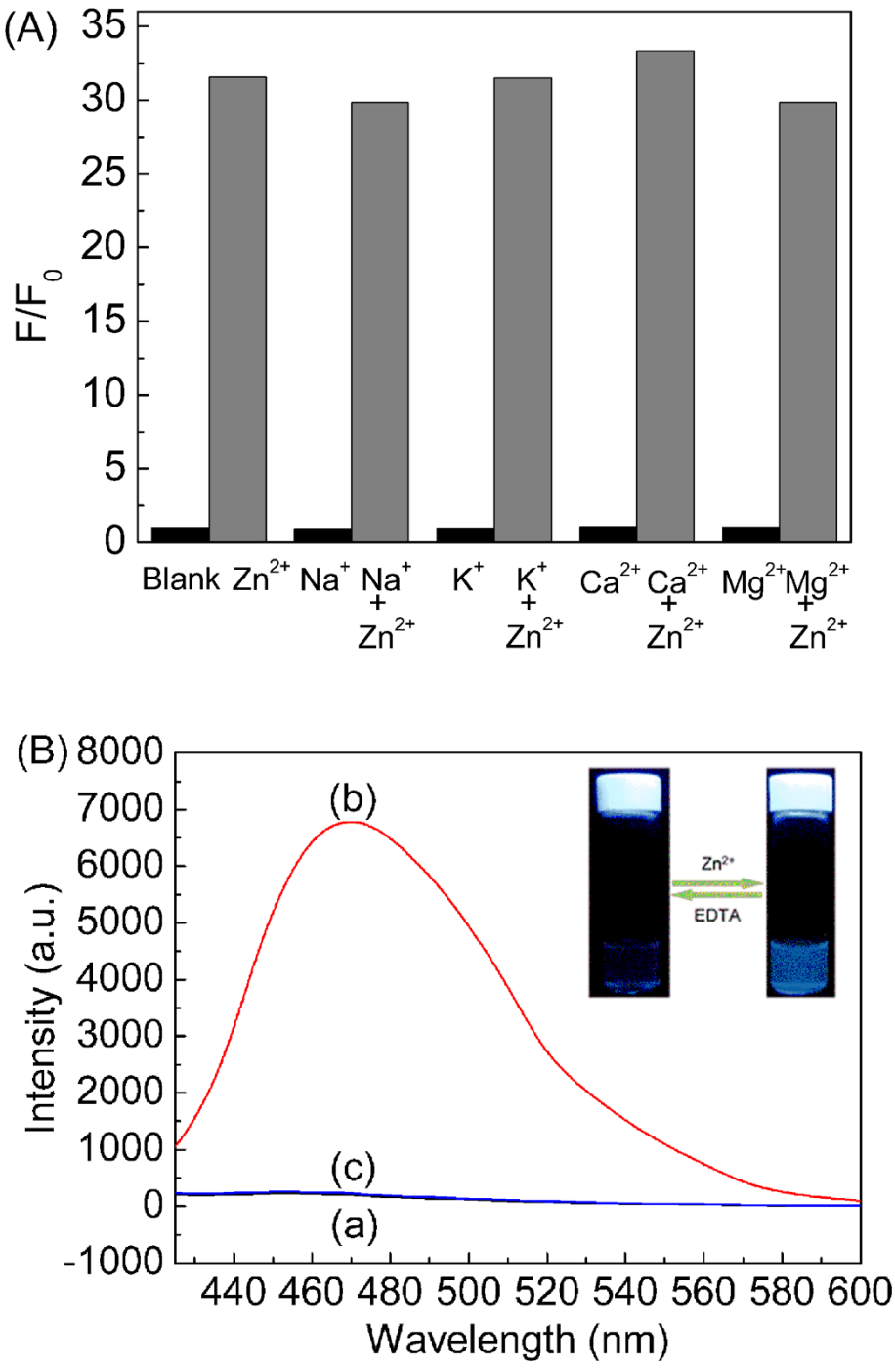

Figure 9 Competition of DTH-Fe_3O_4@SiO_2 towards cations and reversibility of DTH-Fe_3O_4@SiO_2 towards Zn^{2+}. (**A**) Fluorescent emission changes of DTH-Fe_3O_4@SiO_2 (0.3 g/L) upon addition of 1, blank; 2, Zn^{2+}; 3, Na^+; 4, Na^+ + Zn^{2+}; 5, K^+; 6, K^+ + Zn^{2+}; 7, Ca^{2+}; 8, Ca^{2+} + Zn^{2+}; 9, Mg^{2+}; and 10, Mg^{2+} + Zn^{2+} (each metal ion is 100 μM) in ethanol at room temperature. (**B**) Fluorescence spectra of DTH-Fe_3O_4@SiO_2 (0.3 g/L) in (a) without, (b) with Zn^{2+} (1.0×10^{-4} M), and (c) after treatment with EDTA (2.5×10^{-4} M) in (b) solution. The inset picture shows the photograph of DTH-Fe_3O_4@SiO_2 with Zn^{2+} by treatment of EDTA (2.5×10^{-4} M) under a 365-nm UV light.

separation of Zn^{2+} in ethanol. The inorganic-organic hybrid fluorescent chemosensor DTH-Fe_3O_4@SiO_2 was able to recognize and adsorb Zn^{2+} with a selective and sensitive fluorescence response in ethanol. The magnetic separation capability of Fe_3O_4@SiO_2 NPs and the reversibility of the combination between DTH-Fe_3O_4@SiO_2 and Zn^{2+} would also provide a simple route to separate Zn^{2+} from the environment (Figure 6, inset).

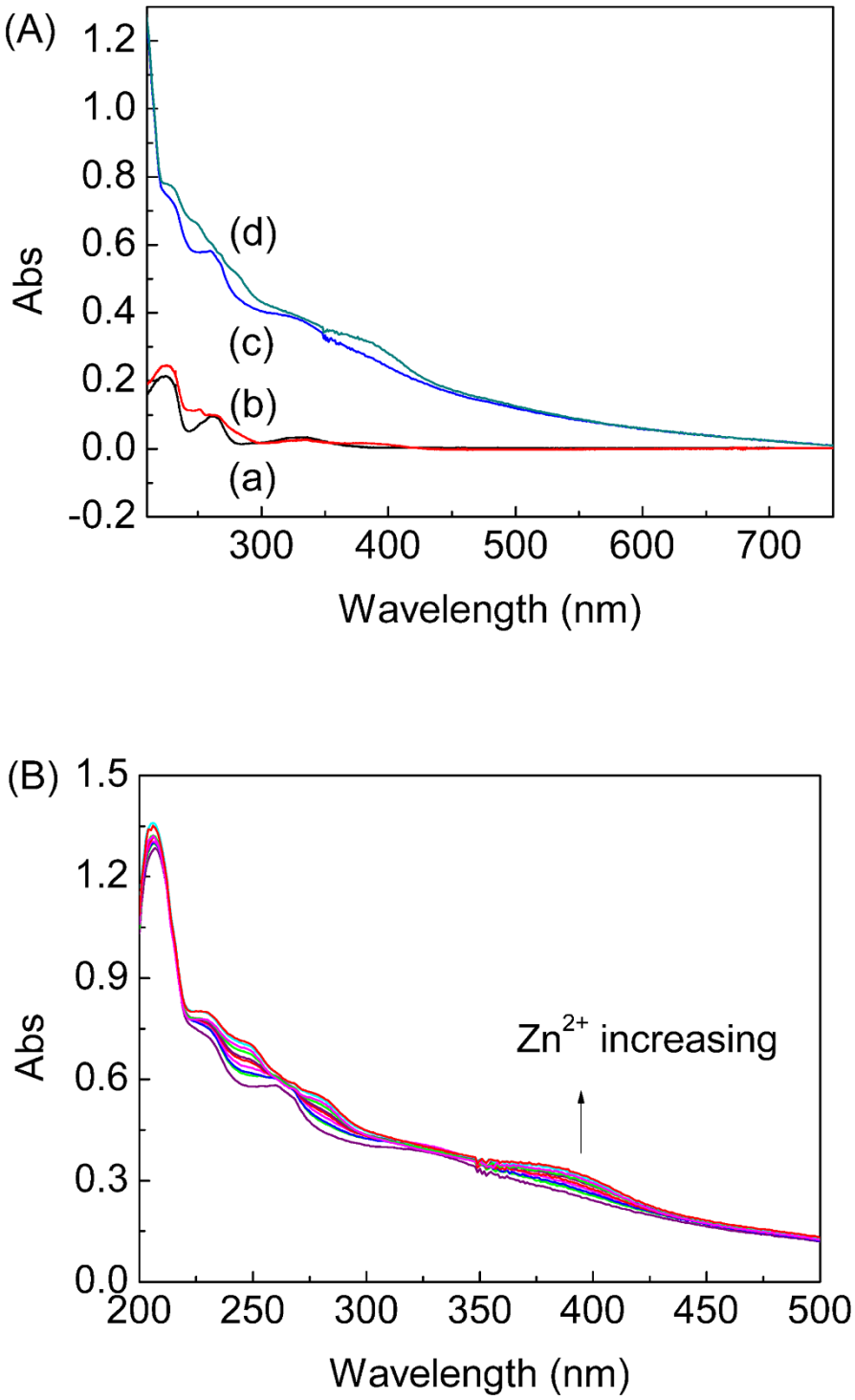

Figure 10 UV-Vis spectra. (**A**) Absorption spectra of (a) DTH-APTES (1.0×10^{-5} M), (b) DTH-APTES + Zn^{2+} (1.0×10^{-4} M), (c) DTH-Fe_3O_4@SiO_2 (0.3 g/L), and (d) DTH-Fe_3O_4@SiO_2 (0.3 g/L) + Zn^{2+} (1.0×10^{-4} M) in ethanol. (**B**) UV-Vis spectra of DTH-Fe_3O_4@SiO_2 (0.3 g/L) in ethanol in the presence of different amounts of Zn^{2+} (0 to 240 μM).

Additional material

Additional file 1: Characterization and properties of DTH-Fe_3O_4@SiO_2. Figure S1, XRD patterns of Fe_3O_4 core; Figure S2, TGA curves of Fe_3O_4@SiO_2 (a) and DTH-Fe_3O_4@SiO_2 (b); Figure S3, selectivity of DTH-Fe_3O_4@SiO_2 for Zn^{2+} in the presence of other metal ions in ethanol; and Table S1, the loading of DTH-APTES in the Fe_3O_4@SiO_2 NPs as estimated by different methods.

Abbreviations

APTES: (3-aminopropyl)triethoxysilane; DLS: dynamic light scattering; DRIFT: diffuse-reflectance infrared Fourier transform; DTH: 3,5-di-tert-butyl-2-hydroxybenzaldehyde; DTH-APTES: 2,4-di-tert-butyl-6-((3-(triethoxysilyl) propylimino)methyl)phenol; EDX: energy-dispersive X-ray spectrometer; NPs: nanoparticles; TEM: transmission electron microscopy; TEOS: tetraethyl orthosilicate; TGA: thermal gravimetric analysis; XRD: X-ray power diffraction.

Acknowledgements

The authors acknowledge the financial support from the NSFC (grant nos. 20931003 and 91122007) and the Specialized Research Fund for the Doctoral Program of Higher Education (grant no. 20110211130002).

Authors' contributions

YW supervised and participated in all the studies and wrote this paper. XP conceived the study and participated in its design. JS participated in the synthesis of the nanoparticles and the testing of fluorescence property. XT, JJ, and WL participated in the revision of the manuscript. All authors read and approved the final manuscript.

Competing interests

The authors declare that they have no competing interests.

Received: 6 July 2011 Accepted: 25 January 2012
Published: 25 January 2012

References

1. Falchuk KH: **The molecular basis for the role of zinc in developmental biology.** *Mol Cell Biochem* 1998, **188**:41.
2. Zalewski PD, Forbes IJ, Betts WH: **Correlation of apoptosis with change in intracellular labile Zn(II) using zinquin [(2-methyl-8-*p*-toluenesulphonamido-6-quinolyloxy)acetic acid], a new specific fluorescent probe for Zn(II).** *Biochem J* 1993, **296**:403.
3. Maret W, Jacob C, Vallee BL, Fischer EH: **Inhibitory sites in enzymes: zinc removal and reactivation by thionein.** *Proc Natl Acad Sci* 1999, **96**:1936.
4. Cuajungco MP, Lees GJ: **Zinc metabolism in the brain: relevance to human neurodegenerative disorders.** *Neurobiol Dis* 1997, **4**:137.
5. Choi DW, Koh JY: **Zinc and brain injury.** *Annu Rev Neurosci* 1998, **21**:347.
6. Bush AI: **Metals and neuroscience.** *Curr Opin Chem Biol* 2000, **4**:184.
7. Miller Y, Ma B, Nussinov R: **Zinc ions promote alzheimer Aβ aggregation via population shift of polymorphic states.** *Proc Natl Acad Sci* 2010, **107**:9490.
8. Duce JA, Tsatsanis A, Cater MA, James SA, Robb E, Wikhe K, Leong SL, Perez K, Johanssen T, Greenough MA, Cho H-H, Galatis D, Moir RD, Masters CL, McLean C, Tanzi RE, Cappai R, Barnham KJ, Ciccotosto GD, Rogers JT, Bush AI: **Iron-export ferroxidase activity of β-amyloid precursor protein is inhibited by zinc in alzheimer's disease.** *Cell* 2010, **142**:857.
9. Li Q, Zhao X, Lv Q, Liu G: **The determination of zinc in water by flame atomic absorption spectrometry after its separation and preconcentration by malachite green loaded microcrystalline triphenylmethane.** *Sep Purif Technol* 2007, **55**:76.
10. Wilhartitz P, Dreer S, Krismer R, Bobleter O: **High performance ultra trace analysis in molybdenum and tungsten accomplished by on-line coupling of ion chromatography with simultaneous ICP-AES.** *Microchim Acta* 1997, **125**:45.
11. Gupta NR, Mittal S, Kumar S, Kumar SKA: **Potentiometric studies of N, N'-Bis(2-dimethylaminoethyl)-N, N'-dimethyl-9,10 anthracenedimethanamine as a chemical sensing material for Zn(II) ions.** *Mater Sci Eng C* 2008, **28**:1025.
12. Xu Z, Baek K-H, Kim HN, Cui J, Qian X, Spring DR, Shin I, Yoon J: **Zn^{2+}-triggered amide tautomerization produces a highly Zn^{2+}-selective, cell-permeable, and ratiometric fluorescent sensor.** *J Am Chem Soc* 2010, **132**:601.
13. de Silva AP, Gunaratne HQN, Gunnlaugsson T, Huxley AJM, McCoy CP, Rademacher JT, Rice TE: **Signaling recognition events with fluorescent sensors and switches.** *Chem Rev* 1997, **97**:1515.
14. Wong BA, Friedle S, Lippard SJ: **Solution and fluorescence properties of symmetric dipicolylamine-containing dichlorofluorescein-based Zn^{2+} sensors.** *J Am Chem Soc* 2009, **131**:7142.
15. Nolan EM, Lippard SJ: **Small-molecule fluorescent sensors for investigating zinc metalloneurochemistry.** *Acc Chem Res* 2008, **42**:193.
16. Zhang XA, Hayes D, Smith SJ, Friedle S, Lippard SJ: **New strategy for quantifying biological zinc by a modified zinpyr fluorescence sensor.** *J Am Chem Soc* 2008, **130**:15788.
17. Zhang Y, Guo X, Si W, Jia L, Qian X: **Ratiometric and water-soluble fluorescent zinc sensor of carboxamidoquinoline with an alkoxyethylamino chain as receptor.** *Org Lett* 2008, **10**:473.
18. Komatsu K, Urano Y, Kojima H, Nagano T: **Development of an iminocoumarin-based zinc sensor suitable for ratiometric fluorescence imaging of neuronal zinc.** *J Am Chem Soc* 2007, **129**:13447.
19. Hanaoka K, Kikuchi K, Kojima H, Urano Y, Nagano T: **Development of a zinc ion-selective luminescent lanthanide chemosensor for biological applications.** *J Am Chem Soc* 2004, **126**:12470.
20. Maruyama S, Kikuchi K, Hirano T, Urano Y, Nagano T: **A novel, cell-permeable, fluorescent probe for ratiometric imaging of zinc ion.** *J Am Chem Soc* 2002, **124**:10650.
21. Zhou X, Yu B, Guo Y, Tang X, Zhang H, Liu W: **Both visual and fluorescent sensor for Zn^{2+} based on quinoline platform.** *Inorg Chem* 2010, **49**:4002.
22. Komatsu K, Kikuchi K, Kojima H, Urano Y, Nagano T: **Selective zinc sensor molecules with various affinities for Zn^{2+}, revealing dynamics and regional distribution of synaptically released Zn^{2+} in hippocampal slices.** *J Am Chem Soc* 2005, **127**:10197.
23. Marshall M, Draney D, Sevick-Muraca E, Olive D: **Single-dose intravenous toxicity study of IRDye 800CW in sprague-dawley rats.** *Mol Imaging Biol* 2010, **12**:583.
24. Herrmann IK, Urner M, Koehler FM, Hasler M, Roth-Z'Graggen B, Robert N, Grass UZ, Beck-Schimmer B, Stark WJ: **Blood purification using functionalized core/shell nanomagnets.** *Small* 2010, **6**:1388.
25. Han WS, Lee HY, Jung SH, Lee SJ, Jung JH: **Silica-based chromogenic and fluorogenic hybrid chemosensor materials.** *Chem Soc Rev* 2009, **38**:1904.
26. Zheng J, Xiao C, Fei Q, Li M, Wang B, Feng G, Yu H, Huan Y, Song Z: **A highly sensitive and selective fluorescent Cu^{2+} sensor synthesized with silica nanoparticles.** *Nanotechnology* 2010, **21**:045501.
27. Lee SJ, Lee J-E, Seo JB, Jeong Y, Lee SS, Jung JH: **Optical sensor based on nanomaterial for the selective detection of toxic metal ions.** *Adv Funct Mater* 2007, **17**:3441.
28. Meng Q, Zhang X, He C, He G, Zhou P, Duan C: **Multifunctional mesoporous silica material used for detection and adsorption of Cu^{2+} in aqueous solution and biological applications in vitro and in vivo.** *Adv Funct Mater* 2010, **20**:1903.
29. Gao L, Wang Y, Wang J, Huang L, Shi L, Fan X, Zou Z, Yu T, Zhu M, Li Z: **A novel Zn^{II}-sensitive fluorescent chemosensor assembled within aminopropyl-functionalized mesoporous SBA-15.** *Inorg Chem* 2006, **45**:6844.
30. Son H, Lee HY, Lim JM, Kang D, Han WS, Lee SS, Jung JH: **A highly sensitive and selective turn-on fluorogenic and chromogenic sensor based on BODIPY-functionalized magnetic nanoparticles for detecting lead in living cells.** *Chem Eur J* 2010, **16**:11549.
31. Park M, Seo S, Lee IS, Jung JH: **Ultraeffcient separation and sensing of mercury and methylmercury ions in drinking water by using aminonaphthalimide-functionalized Fe_3O_4@SiO_2 core/shell magnetic nanoparticles.** *Chem Commun* 2010, **46**:4478.
32. Wang X, Wang P, Dong Z, Dong Z, Ma Z, Jiang J, Li R, Ma J: **Highly sensitive fluorescence probe based on functional SBA-15 for selective detection of Hg^{2+}.** *Nanoscale Res Lett* 2010, **5**:1468.
33. Chai F, Wang T, Li L, Liu H, Zhang L, Su Z, Wang C: **Fluorescent gold nanoprobes for the sensitive and selective detection for Hg^{2+}.** *Nanoscale Res Lett* 2010, **5**:1856.

34. Dong Z, Yang B, Jin J, Li J, Kang H, Zhong X, Li R, Ma J: **Quinoline group modified carbon nanotubes for the detection of zinc ions.** *Nanoscale Res Lett* 2009, **4**:335.
35. Corr SA, Rakovich YP, Gun'ko YK: **Multifunctional magnetic-fluorescent nanocomposites for biomedical applications.** *Nanoscale Res Lett* 2008, **3**:87.
36. Wang B, Hai J, Liu Z, Wang Q, Yang Z, Sun S: **Selective detection of iron (III) by rhodamine-modified Fe_3O_4 nanoparticles.** *Angew Chem Int Ed* 2010, **49**:4576.
37. Bao F, Yao J-L, Gu R-A: **Synthesis of magnetic Fe_2O_3/Au core/shell nanoparticles for bioseparation and immunoassay based on surface-enhanced raman spectroscopy.** *Langmuir* 2009, **25**:10782.
38. Babic M, Horák D, Trchová M, Jendelová P, Glogarová Ki, Lesný P, Herynek V, Hájek M, Syková E: **Poly(L-lysine)-modified iron oxide nanoparticles for stem cell labeling.** *Bioconjugate Chem* 2008, **19**:740.
39. McCarthy JR, Bhaumik J, Karver MR, Sibel Erdem S, Weissleder R: **Targeted nanoagents for the detection of cancers.** *Molecular Oncology* 2010, **4**:511.
40. Taboada E, Solanas R, Rodriguez E, Weissleder R, Roig A: **Supercritical-fluid-assisted one-pot synthesis of biocompatible core (γ-Fe_2O_3)/shell(SiO_2) nanoparticles as high relaxivity T_2-contrast agents for magnetic resonance imaging.** *Adv Funct Mater* 2009, **19**:2319.
41. Guo N, Wu DC, Pan XH, Lu ML: **Magnetic polymer microspheres with azidocarbonyl groups: synthesis, characterization and application in protein immobilization.** *J Appl Polym Sci* 2009, **112**:2383.
42. Nigam S, Barick KC, Bahadur D: **Development of citrate-stabilized Fe_3O_4 nanoparticles: conjugation and release of doxorubicin for therapeutic applications.** *J Magn Magn Mater* 2011, **323**:237.
43. Stöber W, Fink A, Bohn E: **Controlled growth of monodisperse silica spheres in the micron size range.** *J Colloid Interface Sci* 1968, **26**:62.
44. Malumbazo N, Mapolie SF: **Silica immobilized salicylaldimine Cu(II) and Co(II) complexes as catalysts in cyclohexene oxidation: a comparative study of support effects.** *J Mol Catal A: Chem* 2009, **312**:70.
45. Ray S, Mapolie SF, Darkwa J: **Catalytic hydroxylation of phenol using immobilized late transition metal salicylaldimine complexes.** *J Mol Catal A: Chem* 2007, **267**:143.
46. Ma D, Guan J, Normandin F, DeÂnommeÂe S, Enright G, Veres T, Simard B: **Multifunctional nano-architecture for biomedical applications.** *Chem Mater* 2006, **18**:1920.
47. Lin Y-S, Haynes CL: **Synthesis and characterization of biocompatible and size-tunable multifunctional porous silica nanoparticles.** *Chem Mater* 2009, **21**:3979.
48. Laurent S, Forge D, Port M, Roch A, Robic C, Elst LV, Muller RN: **Magnetic iron oxide nanoparticles: synthesis, stabilization, vectorization, physicochemical characterizations, and biological applications.** *Chem Rev* 2008, **108**:2064.
49. Zhang J, Li D, Liu G, Glover KJ, Liu T: **Lag periods during the self-assembly of {$Mo_{72}Fe_{30}$} macroions: connection to the virus capsid formation process.** *J Am Chem Soc* 2009, **131**:15152.
50. Sethi M, Joung G, Knecht MR: **Stability and electrostatic assembly of Au nanorods for use in biological assays.** *Langmuir* 2008, **25**:317.
51. Arita T, Ueda Y, Minami K, Naka T, Adschiri T: **Dispersion of fatty acid surface modified ceria nanocrystals in various organic solvents.** *Ind Eng Chem Fundam* 2009, **49**:1947.
52. Lai C-W, Wang Y-H, Lai C-H, Yang M-J, Chen C-Y, Chou P-T, Chan C-S, Chi Y, Chen Y-C, Hsiao J-K: **Iridium-complex-functionalized Fe_3O_4/SiO_2 core/shell nanoparticles: a facile three-in-one system in magnetic resonance imaging, luminescence imaging, and photodynamic therapy.** *Small* 2008, **4**:218.
53. Ren C, Li J, Chen X, Hu Z, Xue D: **Preparation and properties of a new multifunctional material composed of superparamagnetic core and rhodamine B doped silica shell.** *Nanotechnology* 2007, **18**:345604.
54. Chen L, Xu Z, Dai H, Zhang S: **Facile synthesis and magnetic properties of monodisperse Fe_3O_4/silica nanocomposite microspheres with embedded structures via a direct solution-based route.** *J Alloys Compd* 2010, **497**:221.
55. Mu L, Shi W, Chang JC, Lee S-T: **Silicon nanowires-based fluorescence sensor for Cu(II).** *Nano Lett* 2008, **8**:104.
56. Murthy RSS, Leyden DE: **Quantitative determination of (3-aminopropyl) triethoxysilane on silica gel surface using diffuse reflectance infrared Fourier transform spectrometry.** *Anal Chem* 1986, **58**:1228.
57. Pal P, Rastogi SK, Gibson CM, Aston DE, Branen AL, Bitterwolf TE: **Fluorescence sensing of zinc(II) using ordered mesoporous silica material (MCM-41) functionalized with N-(quinolin-8-yl)-2-[3-(triethoxysilyl)propylamino]acetamide.** *ACS Appl Mat Interfaces* 2011, **3**:279.
58. Song C, Zhang X, Jia C, Zhou P, Quan X, Duan C: **Highly sensitive and selective fluorescence sensor based on functional SBA-15 for detection of Hg^{2+} in aqueous media.** *Talanta* 2010, **81**:643.
59. Sasithorn J, Wiwattanadate D, Sangsuk S: **Utilization of fly ash from power plant for adsorption of hydrocarbon contamination in water.** *J Met Mater Miner* 2010, **20**:5.
60. Kim E, Kim HJ, Bae DR, Lee SJ, Cho EJ, Seo MR, Kim JS, Jung JH: **Selective fluoride sensing using organic-inorganic hybrid nanomaterials containing anthraquinonew.** *New J Chem* 2008, **32**:1003.
61. Sun Y, Liu G, Gu H, Huang T, Zhang Y, Li H: **Magnetically recoverable SiO_2-coated Fe_3O_4 nanoparticles: a new platform for asymmetric transfer hydrogenation of aromatic ketones in aqueous medium.** *Chem Commun* 2011, **47**:2583.
62. Peng X, Tang X, Qin W, Dou W, Guo Y, Zheng J, Liu W, Wang D: **Aroylhydrazone derivative as fluorescent sensor for highly selective recognition of Zn^{2+} ions: syntheses, characterization, crystal structures and spectroscopic properties.** *Dalton Trans* 2011, **40**:5271.
63. Wu Z, Zhang Y, Ma JS, Yang G: **Ratiometric Zn^{2+} sensor and strategy for Hg^{2+} selective recognition by central metal ion replacement.** *Inorg Chem* 2006, **45**:3140.
64. Nolan EM, Burdette SC, Harvey JH, Hilderbrand SA, Lippard SJ: **Synthesis and characterization of zinc sensors based on a monosubstituted fluorescein platform.** *Inorg Chem* 2004, **43**:2624.
65. Xue L, Wang H-H, Wang X-J, Jiang H: **Modulating affinities of di-2-picolylamine (DPA)-substituted quinoline sensors for zinc ions by varying pendant ligands.** *Inorg Chem* 2008, **47**:4310.
66. Sarkar M, Banthia S, Samanta A: **A highly selective 'off-on' fluorescence chemosensor for Cr(III).** *Tetrahedron Lett* 2006, **47**:7575.

doi:10.1186/1556-276X-7-86
Cite this article as: Wang *et al.*: Highly selective fluorescent chemosensor for Zn^{2+} derived from inorganic-organic hybrid magnetic core/shell Fe_3O_4@SiO_2 nanoparticles. *Nanoscale Research Letters* 2012 **7**:86.